European Journal of Computational Mechanics, 2014
Vol. 23, Nos. 3–4, 138–160, http://dx.doi.org/10.1080/17797179.2014.945276

Taylor & Francis
Taylor & Francis Group

On morphing wing for roll augmentation via material fitness using surrogate modelling

Narcis M. Ursache[a]*, Neil W. Bressloff[b] and Andy J. Keane[a]

[a]*Department of Mechanical, Aerospace and Civil Engineering, Brunel University, London UB8 3PH, UK;* [b]*Computational Engineering and Design, Southampton University, Southampton SO17 1BJ, UK*

This research is concerned with the design and analysis of a multi-camber morphing wing that meets prescribed aerodynamic configurations according to the design intent. A global optimisation paradigm is used towards morphing wing that interlinks aerodynamic enhancement via material fitness and efficient structural shape optimisation. A heuristic approach is proposed in this work that combines both airfoil and wing-morphing derivations. Based on non-linear structural solutions, the flexible airfoils allow multiple shape changes through an array of cambers, so that prescribed flow improvements can be achieved. The heuristic argument is then extended towards global shape control of three-dimensional wings with the remit to enhance roll control. The design paradigm employs a hierarchical strategy interleaving model parametrisation with structural optimisation into the aerodynamic analysis; and, in conjunction with global approximation technique, roll augmentation is investigated whilst total drag is minimised.

Keywords: multi-disciplinary optimisation; material modelling; surrogate modelling

1. Introduction

The surge in technological research in new materials and structures provided much scope in bringing to life adaptive structures that can *morph* through an array of shapes and meet requisite environment needs or mimic nature. In real life, such technologies aim at large changes in shape so that some vehicular performance can be augmented, but the limitation comes with the structural stiffness. Morphing aircraft concepts (Roth & Crossley, 2003) rely on actively and continuously changing its shape to adapt it to new flight conditions with the aim of enhancing efficiency, translating thing into the need for an optimum flight envelope, optimised mission segments through smart reconfiguration, improved manoeuvrability, survivability, optimum weight, etc. Aircraft efficiency can also be defined through fully integrated airplane programmes (i.e. design, certification, production, test, delivery, operation, maintenance) within the product life cycle management, through manufacturers and operators effort, as energy or monetary units (Gilyard, Georgie, & Barnicki, 1999) to achieve an acceptable airframe configuration.

Morphing aircraft becomes competitive over conventional aircraft when at least aerodynamic metrics are considered, when different mission tasks and roles are defined (Weisshaar, 2006). Therefore, flow control represents the sine qua non of the aerodynamic morphing concepts, whereby the study of interaction between fluid dynamics and structures become the key drivers in shaping morphing architectures.

*Corresponding author. Email: Narcis.Ursache@brunel.ac.uk

Such technologies can be easily claimed by pioneering military polymorph planes, e.g. the tilt-rotor V-22 Osprey, swing-wing F-111 Aardvark, F-14 Tomcat or B1 Lancer through its variable sweep wing. The difficulties of accommodating additional mechanisms for variable geometries and requisite fuel efficiency make it very difficult to achieve significant advancements in this field.

Since the early 1980s, there have been a plethora of morphing concepts based on fully integrated *smart structures* for performance and shape control of deformable flight devices. Such enhancements for wings are being developed to improve their efficiency in off-design regimes. The adaptive strategies reside in geometry parameters that either have a global effect on shape change, or local, so that flight efficiency is achieved according to the design intent. By and large, morphing applications are mainly governed by intricate topology schemes for global shape control (e.g. smart actuator drivers (Pinkerton & Moses, 1997; Seifert, Eliahu, Greenblatt, & Wygnanski, 1998), compliant mechanisms (Saggere & Kota, 1999), etc.) and for local geometry shape change; flow control devices to tailor the boundary layer prevail (Amitay, Smith, Kibens, Parekh, & Glezer, 2001), or simplistic applied point forces using actuator-based architectures (Rodrigues, 2007; Thuwis, Abdalla, & Gurdal, 2010; Ursache, Keane, & Bressloff, 2006).

From a different perspective, morphing concepts derive certain local unidirectional geometry changes. Some of the morphologies are ubiquitous today (their purpose is to facilitate a wider operational envelope) and some are currently addressed in applications on contemporary aircraft in production as well as future airplane programmes. Such feasibility studies have recorded significant effort towards both civil and military applications through a number of wing-morphing programmes by DARPA/NASA/AFRL and European framework (see SADE, Novemor, Morphing Aircraft, etc.), exploring and exploiting the use of smart materials for actuation (Scherer, Martin, Appa, Kudva, & West, 1997), enhancing manoeuvrability through tailored aerodynamics (Voracek, Pendleton, Reichenbach, Griffin, & Welch, 2003), or a combination of technologies integrated into aircraft structures and aerodynamics (Love, Zink, Stroud, Bye, & Chase, 2004). More variability in shape change by means of combined scheduling and localised multidirectional shape change found applications via bistable composites (Lachenal, Weaver, & Daynes, 2012), aeroelastic tailoring (Li, Guo, & Xiang, 2012; Thuwis, 2012) or morphing winglets (Ursache & Mares, 2012; Ursache, Melin, Isikveren, & Friswell, 2007).

By and large, morphing concepts targeting large geometry changes are associated with theories based on non-linear post-critical structural deformation (Barrett & Vos, 2007; Ursache et al., 2006) or by means of mechanisms (Saggere & Kota, 1999; Ursache & Mares, 2012). Herein, means to provide global wing shape changes are based on a rather simplistic control law in order to improve upon wing aerodynamic properties with the benefit of low powered actuation control. Based on similar control approach, i.e. spinal structures, this paper investigates the morphing methodology through material fitness and global approximation technique in order to tailor airfoil flow characteristics and overall wing roll control. Such analyses interlink sequences of parametrisation with structural analysis and aerodynamic assessment within a response surface framework in lieu of direct searches. The main goal of this approach is to provide a conceptual wing shape adaptability that relies on low-power actuation system.

2. Hyperelastic material fitness

The design methodology proposed in this paper for morphing applications is based on the concept of spinal structures (Ursache, Bressloff, & Keane, 2004; Ursache et al.,

2006), involving both structural and aerodynamic optimisation with respect to the geometry of the airfoils under different flow conditions. By making use of non-linear structural responses, camber control of deformable airfoils can be achieved by using a carefully designed preloaded internal spinal structure (see Figure 1) that moves through the desired shape changes under the control of a single actuator, delivering aerodynamic characteristics that match a set of pre-specified target shapes. The actuation control law is based on eccentrically loaded slender structures operating in the post-buckling regime in order to achieve large deflections with only modest incremental load changes.

In the current study large deformations of the strut occur (i.e. up to 10–15% chord in the post-critical regime) and it was assumed that the thickness distribution of the deflected airfoil using the spinal structure (Ursache et al., 2006) kept its analytical definition throughout the deformation. In reality, the constitutive hyperelastic models are phenomenological and may affect the structural strength of the set-up. Therefore, a low-density elastomeric foam is studied here to simulate a true mechanical response, to bring closure to the initial assumption on deformation simplicity of the fixed thickness distribution. A comprehensive overview on the potential materials along with the test beds can be found in Kikuta (2003).

2.1. Overview of hyperelasticity

Hyperelastic materials and especially, elastomeric foams have a wide range of applicability in industry, ranging from biomedical engineering (e.g. arterial stents, artifical heart valves) to sport engineering and also the vehicle industry (e.g. suspension), mainly because of their excellent energy absorption and moulding capabilities. The constitutive law admits a continuous potential function that can control the stress–strain responses through the 'performance' parameters. The hyperfoams are cellular materials that can deform elastically up to 90% in compression, and also allow for large volumetric deformation (i.e. the effective Poisson ratio is less that .45–5) due to their porosity.

The linear elastic constitutive laws can only be used for linearised strain-stress relationships, under the assumption of small deformations. However, there are complex models where small strains (e.g. soils) and also finite strains (e.g. polymers) can be analysed on a elastic foundation, but exhibit non-linear stress–strain behaviour. The emergence of non-linear constitutive laws begun nearly 60 years ago when exact non-linear solutions to incompressible isotropic material problems (i.e. hyperelasticity) were found due to Rivlin's discovery (Rivlin, 1948). Hyperelasticity comprises both non-linear material response and non-linear kinematics, with applications in both incompressible (i.e. rubber like material) and highly compressible (i.e. elastomeric foam) responses.

The main features of the mechanical behaviour on hyperelastic materials are that (1) the material behaviour is elastic (i.e. there is no history dependence of stress, in addition to the reversibility assumption); (2) the material is temperature dependent in

Figure 1. Structural set-up for morphing airfoil camber.

shear (i.e. that heat causes stiffening); (3) the shear modulus is very small compared to that of metals; (4) an isotropy assumption (i.e. the molecular chain, although randomly distributed in the mass of the material, exhibits deformation in the direction of straining).

Since hyperelastic materials exhibit large deformations over a wide range of compressibility, a suitable form of the strain-energy functional has been proposed by Ogden (1972) for low-density foams, derived from slightly compressible rubber definitions, including terms of the strain invariants and principal stretches. The elastic behaviour of the foam is based on a modified Hill strain energy function:

$$U = \sum_{i=1}^{N} \frac{2\mu_i}{\alpha_i^2}\left[\widehat{\lambda}_1^{\alpha_i} + \widehat{\lambda}_2^{\alpha_i} + \widehat{\lambda}_3^{\alpha_i} - 3 + \frac{1}{\beta_i}(J_{el}^{-\alpha_i\beta_i} - 1)\right], \tag{1}$$

defined by $\widehat{\lambda}_i = J_{th}^{-\frac{1}{3}}\lambda_i$, where λ_i are the principal deviatoric stretches that give a measure of relative elastic volume $J_{el} = \widehat{\lambda}_1\widehat{\lambda}_2\widehat{\lambda}_3$ ($J_{el} = 1$ for incompressibility) and also the total volume ratio J (i.e. current volume divided by original volume) is defined as temperature variant through the thermal strain ϵ_{th}:

$$J_{el} = \frac{J}{J_{th}} = \frac{1}{J_{th}}\frac{\delta V}{\delta V_0}, \tag{2}$$

$$J_{th} = (1 + \epsilon_{th})^3. \tag{3}$$

Here, μ_i, α_i and β_i are the material parameters to fit experimental data and define the initial shear modulus μ_0 by shear modulus coefficients μ_i,

$$\mu_0 = \sum_{i=1}^{N} \mu_i, \tag{4}$$

where β_i specifies the shape of the volumetric response, being related to the effective Poisson ratio v_i defining the initial bulk modulus K_0

$$K_0 = \sum_{i=1}^{N} 2\mu_i\left(\frac{1}{3} + \beta_i\right), \tag{5}$$

$$\beta_i = \frac{v_i}{1 - 2v_i}, \tag{6}$$

and α_i represents the shape of the stress–strain curve, i.e. a low α increases the curvature of the response and produces a rapid initial compression and stiffening.

A direct search of parameters on structural behaviour of hyperelastic models is also present in the literature, for instance, Twizell and Ogden (1983) and Ogden, Saccomandi, and Sgura (2004), derive a benchmark of non-linear least squares fit (i.e. optimisation) on experimental data, outlining the non-singular optimal solutions to such problems.

3. Airfoil analysis

The elastic properties of elastomeric foams are highly dependent upon the stiffness of the cellular chain and its structural density (Gibson & Ashby, 1977). Since the experimental test data for the material in terms of stress-nominal strain pairs in combinations

of uniaxial, planar, simple shear and volumetric expansion are not provided, the hyperfoam material properties can be tackled using direct input of coefficients into the potential function, to predefine the mechanical response of the model. Both hyperelastic and elastomeric foams have their constitutive laws implemented in several industry commercial non-linear Finite Element Method (FEM) codes, such as Abaqus®/Standard. That enables the user to choose the functional parameters and the order N, so that a mechanical response of the material can be tailored. Here, an inverse design method is approached as discussed in Ursache et al. (2006) and Ursache, Bressloff, and Keane (2011), whilst a functional defined in terms of aerodynamic properties of the deformed set-up is assessed using VGK (VGK, 1997).

3.1. *Problem set-up*

The current section improves upon the equivalent implicit correlation between the deflected strut and the theoretical airfoil surface, providing a more practical approach of the set-up, i.e. a hyperelastic material intrinsically linked to the camber-like strut. Since, a priori knowledge of the proposed material is not provided, an optimisation of the material parameters is carried out via an inverse procedure, using a parent-based search engine (i.e. a GA).

The thickness distribution is represented now by an elastomeric foam constitutive law. A four-digit NACA definition is used to represent the aerodynamic shape of the airfoil in its undeformed state. During the deformation, volumetric changes along with compression–tension states are allowed to occur (n.b., the effect of undesirable ripples and bulges is to be minimised as secondary effect during optimisation) so that good aerodynamic features can be achieved. Therefore, a functional related to the aerodynamics of the set-up is to be minimised and can be stated as follows:

$$\text{Minimise} \quad f(\mathbf{x}) = \|\mathbf{C_p}(\mathbf{x})^t - \mathbf{C_p}(\mathbf{x})\|, \tag{7}$$

$$\text{Subject to} \quad g_i(\mathbf{x}) = d\tau : d\epsilon > 0, \tag{8}$$

$$\mathbf{x} \in \mathbf{X}, \quad \forall j \in \{1, \ldots, n_p\},$$

where $\mathbf{X} = \{\mathbf{x} \in \Re^n \,|\, x \equiv \{\mu_k, \alpha_k, \beta_k\},\ k = 1, \ldots, N\}$ with N the order of the material. The objective function $\mathbf{C_p}(\mathbf{x})$ represents the computed pressure distribution field over a deflected airfoil and is to be matched to a target one $\mathbf{C_p}(\mathbf{x})^t$.

The implicit constraint g_i is defined by the Drucker stability check (i.e. intrinsic to the FEM solver) and is evaluated at each load increment i until the maximum number of increments n_{inc} is reached, to reduce the computational burden of the optimisation. The constraint can be expressed with respect to increments of the principal Kirchhoff stress $d\tau$ following a non-specified principal logarithmic strain $d\epsilon = d(\ln \lambda)$:

$$d\tau : d\epsilon > 0. \tag{9}$$

or as positiveness of the tangential stiffness matrix $\mathbf{D}$ in Krichhoff-Cauchy stress relationship $d\boldsymbol{\tau} = Jds$:

$$d\epsilon : \mathbf{D} : d\epsilon > 0. \tag{10}$$

A number of papers in the literature deal with the estimation of the constitutive parameters of elastomeric foams, searching for rather discrete values that can fit different

experimental data. Such research emphasises that a higher order N of the model coupled with a inconsistent choice of the parameters may lead to high sensitivity, instabilities or a poor fit to the experimental data. Mills and Gilchrist (2000) established consistent agreement to the stress–strain response curve of a second-order low-density polymer using pairs (α_i, μ_i) of discrete values to quantify tensile (e.g. $\alpha_2 = 20$) and compressive (e.g. $\alpha_2 = -2$) hardening coefficients at high strains while intermediate values increase the strain rate in uniaxial compressive response, commenting that first-order model lead to a poor fit of the material.

Therefore, for the current model, an elastomeric foam material with the order of the series expansion $N = 2$ is chosen, to ensure sufficient flexibility and stability of the constitutive law in modelling the structural behaviour of the foam. The elastomeric allows for high compressibility (i.e. flexibility), enabling small reactions of the foam on the camber-like spinal structure in an optimum configuration. The lateral deflection of the beam for larger cambers becomes controllable (as depicted later in Figures 8 and 9), since the hardening behaviour is driven by physical arguments in the outlined functional. The optimisation here accounts for large strains and rotations, since the structural solution is found employing an iterative-based non-linear procedure.

Although in previous optimisation schemes (Ursache et al., 2004), the structural constraint was expressed in terms of bounds for maximum deflection achievable, only the solution (i.e. load–displacement discrete values) represented by a minimum norm to the bound is chosen. The norm can range up to a maximum increment size, which often varies between .001 and .1% of the final solution achieved. Such a norm can also be expressed as change in the displacement field when using a set-up comprising of the beam and the elastomeric foam for 5 and 10% camber to chord ratio. As expected, the gradient deformation is larger at the position of the maximum camber due to the augmented stiffness of the set-up in the presence of the foam.

The global optimisation in this section is based on a structural set-up and flow conditions ($M = .78$). The optimal aerodynamic shapes of the computed airfoils are plotted against the target ones for both 5 and 10% cambers in Figure 2 showing a good agreement which is highlighted in Figure 6 by means of residuals, i.e. the difference between the optimised and target-deflected states. Lack of fitness chordwise prevails towards the leading edge at high camber deflection due to intricate geometry definition of the airfoil. The residuals are minimised towards the trailing edge due to quasi-liniarised geometry (Figure 3).

The aerodynamic properties of the airfoils are sensitive to the perturbations in the aerodynamic shape, but the proposed model, studied over a wide range of flows, indicates a very good agreement in terms of pressure distribution, including mild shock position (see Figure 4 for 5 and 10% cambered airfoils). This agreement is complemented by a linear $C_L - \alpha$ variation over the range of computed incidences, with higher variations of drag towards the end of the Mach-incidence envelope (Figure 5), where shocks are likely to occur but not captured by VGK. The drag polars also outline the true aerodynamic feature of the model, yielding a very similar drag performance to the target shape (Figure 6).

The optimised set of the hyperfoam potential parameters for the underlying model is compared with a number of valid models from the literature, to check its validity within a wide design space encapsulated by experimental data. Here, the validity basis is set by the studies of fitting constitutive parameters to experimental data provided by Mills and Lyn (2001) and Schrodt, Benderoth, Kühhorn, and Silber (2005), for hyperfoams of order $N = 2$. The resulting materials based on the fitted experimental data from

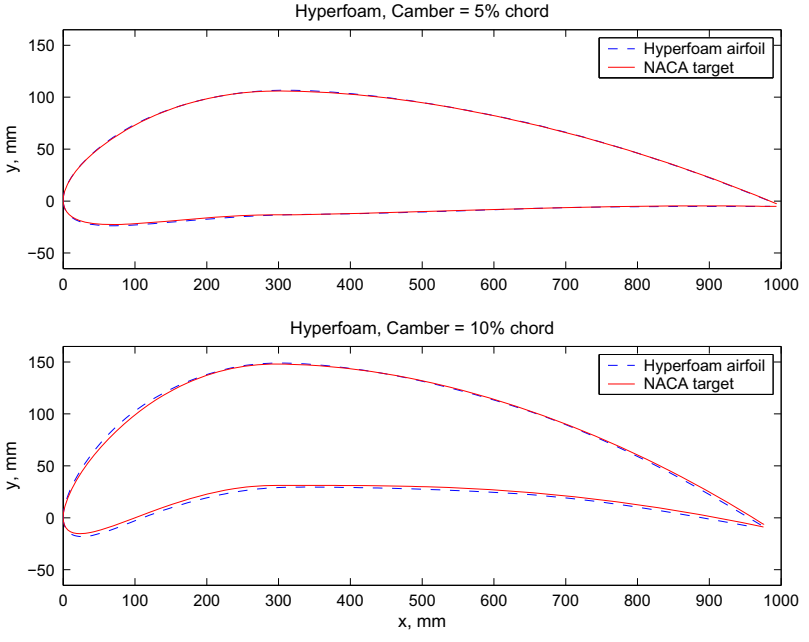

Figure 2. Optimal analytical and experimental airfoils.

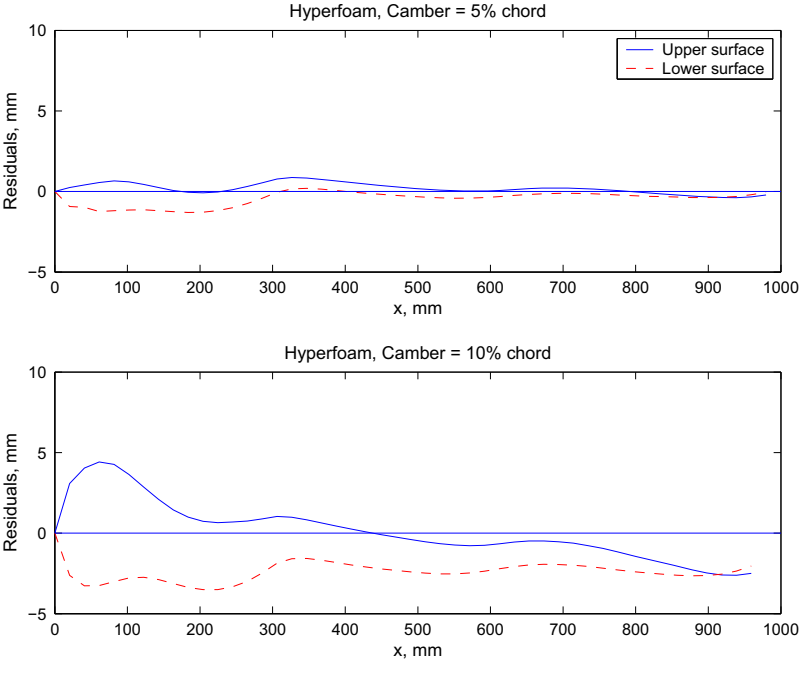

Figure 3. Residuals between optimised hyperfoam and target airfoils in the range of deflection states of 5 and 10%.

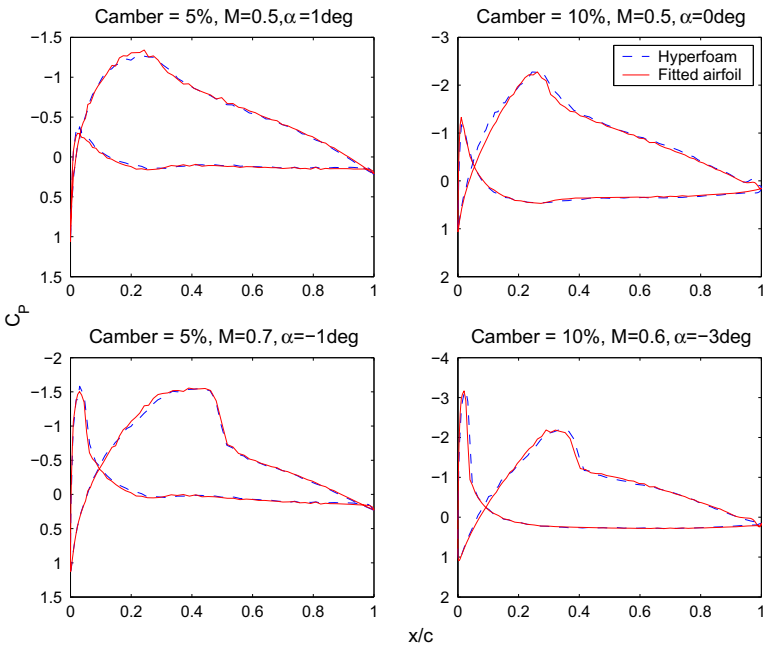

Figure 4. Pressure distributions of 5 and 10% hyperelastic airfoils.

Table 1 are analysed in Figure 7 for camber of 10% chord at Mach .5 and incidence −1°. Clearly, the pressure distributions of the hyperfoam airfoils are intrinsically linked to the structural response of the foam-core, a priori determined by the potential definition in uni-biaxial compression and tension and shear, so that to fit a target. The numerical fitness of the studied hyperfoams is presented here as a root mean square error (see Table 1). The optimised hyperfoam presents a good trade-off between the experimental configurations and exhibits a better fitness with the constitutive parameters close to experimental ones, by controlling the potential definition, thus the stress–strain curve through the μ_i, α_i and v_i parameters.

Qualitatively, the performance of the elastomeric foam can also be emphasised using stability conditions within the constitutive law. Here the design space is large and for constitutive constants highly negative, leading to nominal strain range of $-.9 \leq \epsilon_1 \leq 9$ (the material is prone to instabilities), Abaqus® performs data checks for nine forms of loading: uni-biaxial, shear, planar and volumetric tension and compression and issues warnings for minimum strain, for which the instability is observed.

The physical arguments of the potential from which stress states are derived have a large impact on the local structural behaviour of the foam. The optimal solution here presents an inhomogeneous stress field (Figure 8) and the contours are rather bunched in the radial direction. Concentration factors outlined by large consecutive variation of stiffness (i.e. the discrete thickness distribution scheme used to represent the strut) constitute the origin for small stress concentrations, that 'weed out' with large deflections and also change with the bending curvature of the strut. The inhomogeneous stress field also captures the vertical component of the Cauchy stress tensor s_{33} towards the leading edge, where the stiffness of the foam decreases. The maximum vertical stress for 10%

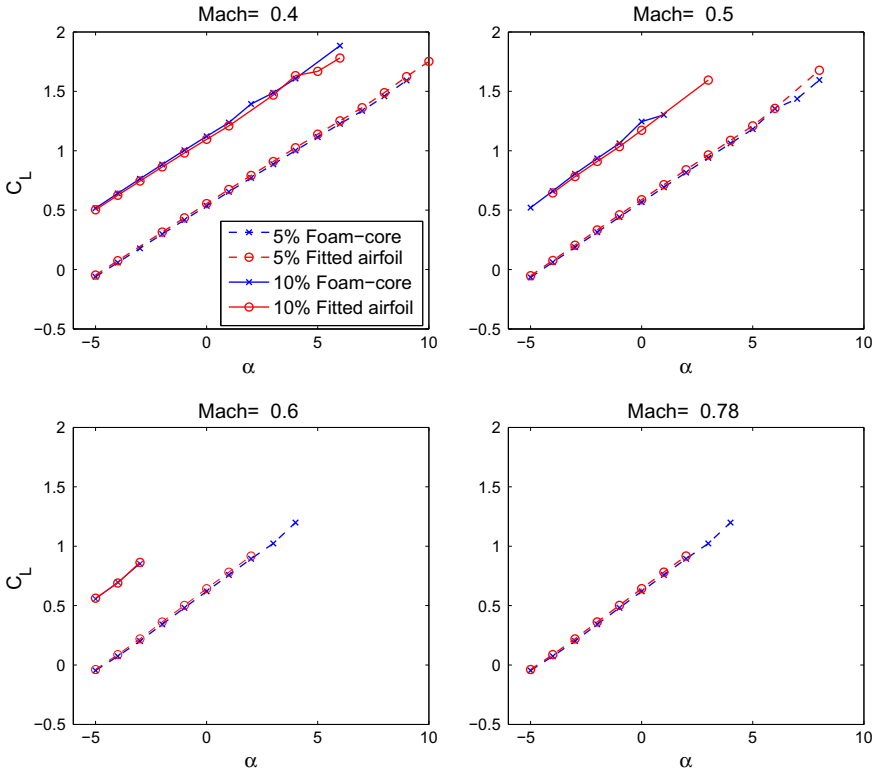

Figure 5. Aerodynamic properties of 5 and 10% hyperelastic airfoils.

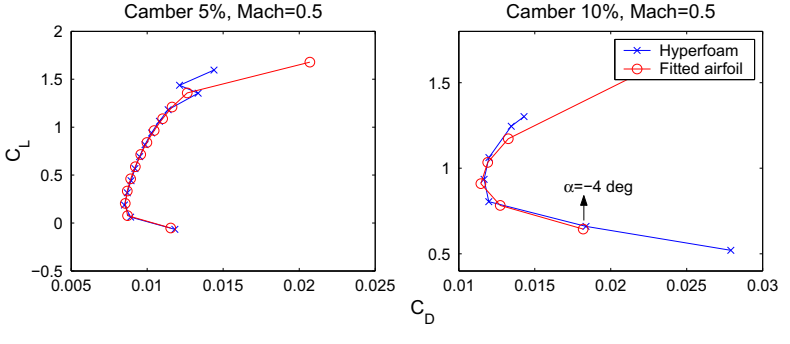

Figure 6. Drag polars of 5 and 10% hyperelastic airfoils.

camber $s_{33} = 34$ kPa, i.e. very low compared to stresses in a shoe-cushioning system (Thomson et al., 1999) ($N = 1$) of 80 kPa or 70 kPa in an impact of a head form on crash mats (Lyn & Mills, 2001) ($N = 2$). The main feature of elastomeric foams concerns the compressibility and this is depicted in Figure 9. The maximum logarithmic compression strain for the 10% cambered airfoil LE_{22} is on the order of −.0239, which is equivalent to a stretch of $\lambda = e^{-.0239}$ or a nominal compressive strain of 2%.

Table 1. Parameters for the hyperfoam materials with $N = 2$.

	Optimised set	Mills and Lyn (2001)	Schrodt et al. (2005)
μ_1	.041280	.018	.00481
α_1	16.021013	8	19.8
μ_2	.246407	.012	.00360
α_2	7.457265	−2	19.8
v_1	.340440	0	.014091
v_2	.273473	.45	.006416
RMSE	.0772824	.123	.158537

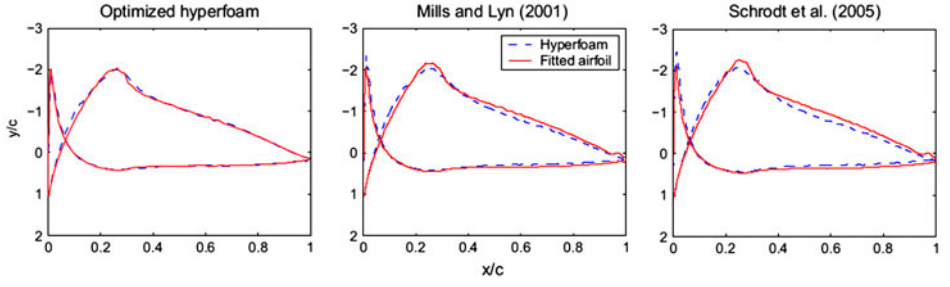

Figure 7. Comparison of pressure distributions of different fitted hyperelastic airfoils for cambers = 10% chord at $M = 0.5$ and $\alpha = 1°$.

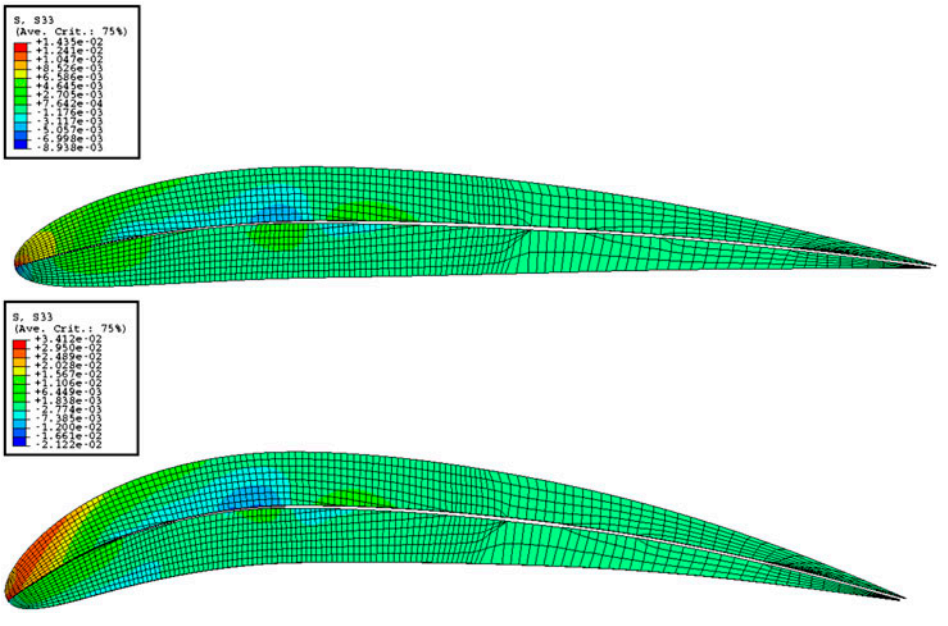

Figure 8. Stress contours of hyperlastic airfoil.

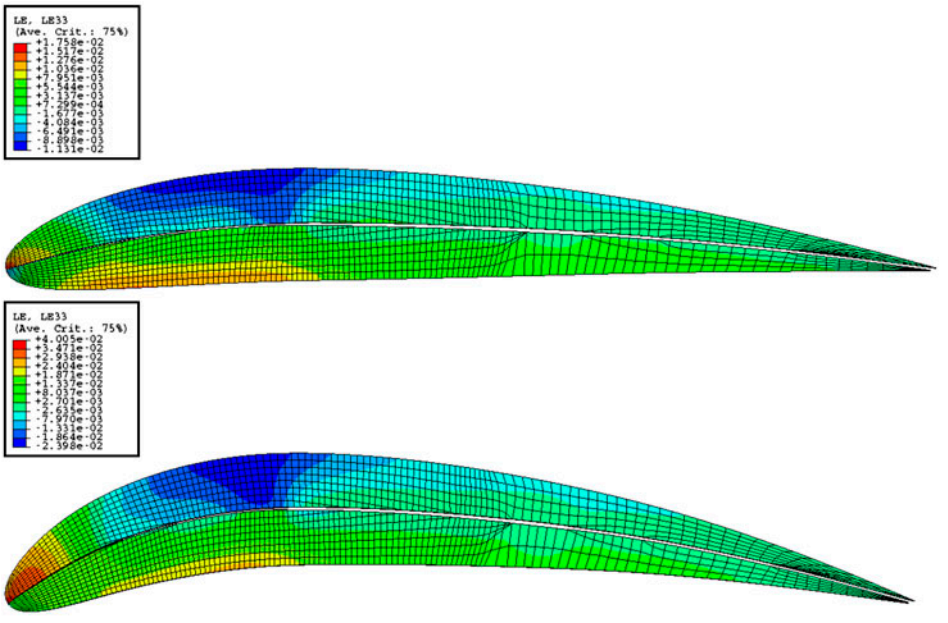

Figure 9. Strain contours of hyperlastic airfoil.

Similarly, $LE_{11} = -.09323$, which leads to a nominal strain of 9%, indicating a mild axial compression of the foam. These invariants predicts the behaviour of the foam with respect to the stress–strain equilibrium path, as for strains smaller than 5%, linear elastic deformations occur due to bending of the cells, followed by a plateau at almost constant stress due to elastic buckling of cell walls.

3.2. Static aeroelastic study of morphing airfoils

A static aeroelastic study of the structurally optimised airfoils is conducted following a loosely coupled and modular method (Alonso, LeGresley, van det Weide, Martins, & Reuther, 2004; Cai & Liu, 2001). The interaction between fluid and structures can be achieved through a wide variety of mapping algorithms (a comprehensive review of such interpolating schemes can be found in Smith, Hodges, and Cesnik (1995)). In the loosely coupled approach, the boundary interface between the two disciplines has a dual character, providing means of mapping the pressure field onto the structural grid (computed by FEM solver), and also interpolating the displacement field into the Computational Fluid Dynamics (CFD) grid. To obtain an aeroelastic solution, these two mappings are repeated and updated in an iterative manner until a convergence criterion is satisfied.

Static aeroelasticity requires geometry conservation through the mapping of the conservative aerodynamic loads f_a, which becomes intrinsic when, under a relaxation procedure, the pressure field is updated with the current and the previous states (Alonso et al., 2004; Cai & Liu, 2001). The updating process is controlled by a relaxation factor, β, that determines the magnitude of the pressure perturbation (i.e. oscillatory), such that:

$$f_a^n = f_a^{n-1} + \beta(f_a^n - f_a^{n-1}), \tag{11}$$

$$0 < \beta < 1.$$

A canonical example consisting a 5% cambered airfoil with optimised cladding is studied under moderate flow conditions with $M = .5$ and $\alpha = 2°$. The airfoil under investigation is subject to similar boundary conditions, whereby the leading edge is pinned and the trailing edge slides, so that full postbuckling regime of the strut and cladding can be captured by the Finite Element Application (FEA) and the extra stiffness from the hyperfoam can be accounted for. The structural set-up consist the best solution from the previous global search including boundary conditions, and the pressure distribution is mapped onto the structural grid so that lift and drag are accounted for (n.b., on a unit width beam, the pressure is discretised into equivalent concentrated forces orthogonal to the aerodynamic surface and applied on the structural boundary-fitted grid). The conversion factor that tunes the pressure distribution also takes into account the width of the beam (i.e. 8 mm), so that the aeroelastic updates are based on full structural strength of the beam and hyperfoam.

In the aeroelastic cycle, the convergence of the solution is accelerated when large relaxation factors are used. Such trends can be seen in Figure 10 for the airfoil, where a relaxation sensitivity study shows the convergence of the solution in the aeroelastic cycle in terms of perturbation f_a (i.e. the non-regular C_P distribution mapped onto the structural-fitted grid and integrated over the width of the beam). For a relaxation factor $\beta = .6$, the aeroelastic solution converges after 15 iterations, whereas for $\beta = .2$, 35 iterations are needed, after which the system becomes self-equilibrated under aeroelastic forces and the convergence criterion is met.

The convergence history in terms of perturbation in Figure 10 shows large oscillations due to the incremental-iterative FEM procedure. The difference between two consecutive incremental solutions can be large which may lead to large oscillations in aerodynamic properties. This variation is intrinsically dictated by the non-linear solution and has a magnitude of an increment. Structural instabilities may also occur, in which case the relaxation factor is augmented by one per cent so that the perturbation to the system is augmented, thus obtaining a stable solution. The convergence history also

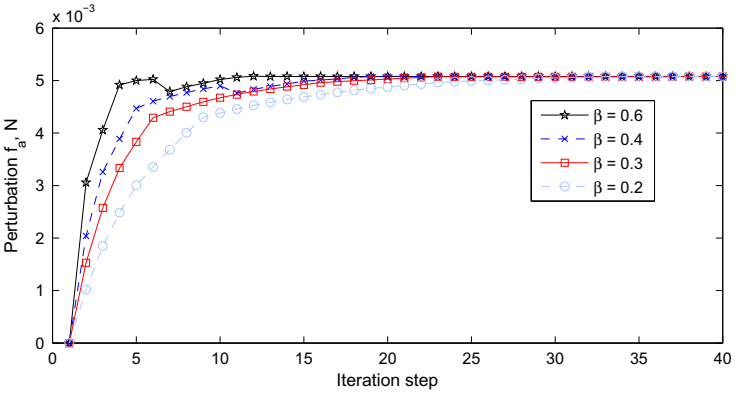

Figure 10. Aeroelastic convergence studies, with different relaxation factors β.

shows that the aeroelastic solution is only slightly changed from the rigid steady state one, with a maximum of one per cent, which proves the airfoil is stiff enough to preserve its optimised rigid state properties under modest impact of extra stiffness due to cladding. This translates into a small variation in requisite actuation force of .5%, whilst airfoil deformation becomes insignificant to affect local flow.

4. Wing analysis

An application of the proposed wing-morphing methodology to transonic wing design for a narrow body aircraft wing is considered here (see Figure 11). The design paradigm is based on a three-dimensional spinal structure by means of a plate model (an orthogonal extension of the two-dimensional model previously analysed), subject to the actuation control law (Ursache et al., 2006) whereby global shape control of the new spinal structure is possible, through offset point loads at the extreme sections of the controllable outboard wing patch, as outlined in Figure 11.

Through stiffness tailoring of slender structures, morphing through a range of cambered shapes defining prescribed airfoils becomes possible and enables large changes in shape by exploiting a range of incremental non-linear structural solutions under eccentric loading whilst meeting prescribed flow characteristics (Ursache et al., 2006, 2011).

Large changes in wing structural shape can have a dramatic effect on the aerodynamic performance of the wing, therefore the optimisation problem becomes multi-objective by nature, with both aerodynamic- and structural-related cost functions and constraints. The geometry of the underlying spinal structure is characterised by a fixed planform and uses two patches, viz. inboard and outboard (see Figure 11). In order to derive a structural set-up that delivers tailored aerodynamic performance with aircraft roll metrics, for simplicity, the outboard wing patch is chosen to be the active element (i.e. linearly actuated) during morphing.

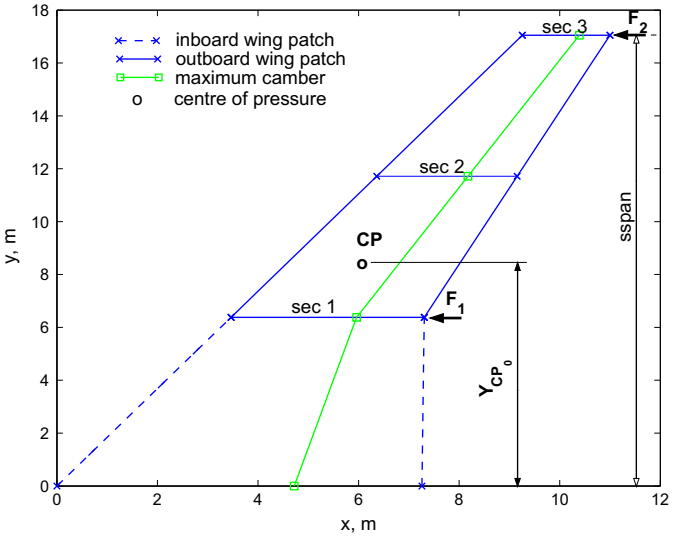

Figure 11. Wing planform with typical inboard and outboard patches. The highlighted outboard wing patch is actuated by point forces at the trailing edge of grid sections ‘sec 1’ and ‘sec 3’. Structural-related objectives are applied to the sections ‘sec 1’, ‘sec 2’ and ‘sec 3’.

Therefore, the underlying model is designed to enhance roll control over the wing and also to maintain the aerodynamic integrity. These two issues are tackled in a single heuristic objective, f_1 (see Equation (12)), by minimising the drag gradient with respect to the position of centre of pressure so that the feasible design solutions encounter low drag for a large change of centre of pressure towards the tip for augmented roll. The flow performance is highly sensitive to the smoothness of the aerodynamic shape of the wing, controlling somewhat the pressure distributions (Scherer et al., 1997), and thus, the overall aerodynamic performance of the wing. Such considerations lead to additional aerodynamic and structural objectives (see Equation (13)) and constraints (see Equations (14)–(18)), so as to aerodynamically maintain product integrity, by enabling the morphed outboard surface to smoothly blend the controlled prescribed sections (note that the sections on which the structural related objectives are studied here are the crank, tip and mid-outboard path positions, i.e. 'sec 1', 'sec 2' and 'sec 3', respectively). This translates into the use of a target wing shape, a priori generated by four-digit NACA airfoils with significant aft camber (i.e. 65% chord), so as to alleviate the inherent transonic flow issues over the wing and also, to avoid spurious designs (to keep to the spirit of the two-dimensional approach).

The smoothness of the structural design is imposed by the objectives f_{sec} on the grid sections highlighted in Figure 11 (i.e. 'sec 1', 'sec 2' and 'sec 3', corresponding to the crank, tip and mid section outboard patch), using metrics that define the fitness of the morphed airfoils (sections) to equivalent NACA airfoils (n.b., implicit four-digit NACA airfoil definition is chosen due to its analytical simplicity and the aerodynamic compromise is assumed). The fitness is defined by the L_2-norm of the difference between the deflected shape $\mathbf{w}(\mathbf{x})$ and its associated explicit target $\mathbf{w}(\mathbf{x})^t$ based on chord, magnitude and position of maximum deflection of deformed sections (note that, this *inverse approach* works towards a given shape by attempting to push some derived characteristic towards a desired configuration). The aerodynamic constraints g_1 and g_2 are expressed with respect to a baseline wing geometry (Ursache et al., 2011) (i.e. constant 2% camber spanwise), and structural constraints g_3 and g_4 control the upper and lower bounds of the displacement field of the crank and tip sections and g_5 controls the maximum yield stress criterion for the material. Therefore, the multi-objective optimisation problem can be stated as follows:

$$\text{Minimise} \quad f_1(\mathbf{x}) = \frac{d\bar{C}_D}{dY_{cp}}, \tag{12}$$

$$f_{\text{sec}}(\mathbf{x}) = \|\mathbf{w}^t - \mathbf{w}\|_2^{\text{sec}}, \tag{13}$$

$$\text{Subject to} \quad g_1(\mathbf{x}) = C_{L_0} - C_L < 0, \tag{14}$$

$$g_2(\mathbf{x}) = Y_{cp_0} - Y_{cp} < 0, \tag{15}$$

$$g_3(\mathbf{x}) = \max|_j \; w_j - a_2 \leq 0, \quad \text{at sec 1}, \tag{16}$$

$$g_4(\mathbf{x}) = a_1 - \max|_j \; w_j \leq 0, \quad \text{at sec}\, 3, \tag{17}$$

$$g_5(\mathbf{x}) = \max|_{\sigma_{Mises}} - \sigma_Y \leq 0, \tag{18}$$

$$\mathbf{x} \in \mathbf{X}, \quad \forall j \in \{1, \ldots, n_p\}, \quad \forall \text{sec} \in \{1, 2, 3\},$$

with $\bar{C}_D = C_D \cdot sspan$, $\mathbf{X} = \{\mathbf{x} \in \Re^n | x_k^{\min} \leq x_k \leq x_k^{\max},\ k = 1, \ldots, n_v\}$ with $x_k^{\min}$ and $x_k^{\max}$ bounds on the n_v structural variables set by the user ($x_k^{\min} = .2$ mm and $x_k^{\max} = 8$ mm for control points, $x_k^{\min}|_{F_1} = -5 \cdot 10^3$ N, $x_k^{\min}|_{F_2} = -100 \cdot 10^3$ N, $x_k^{\max}|_{F_1} = 1 \cdot 10^3$ N and $x_k^{\max}|_{F_2} = -1 \cdot 10^3$ N (Ursache et al., 2006)); w_j are the deflections at the structural position j at final load increment for each of the three sections s considered defined by n_p structural grid points, and $a \in \{a_1, a_2\}$ with $a_1 = g_3(\mathbf{x})$ define the lower and upper displacement bounds for crank 'sec 1' and tip 'sec 3' sections. The increments $d\bar{C}_D = \bar{C}_D - \bar{C}_{D_0}$ and $dY_{cp} = Y_{cp} - Y_{cp_0}$ are computed with respect to baseline geometry characteristics (i.e. $\bar{C}_{D_0} = .015402$, $Y_{cp_0} = 7.5$ m and $C_{L_0} = .51$) (Keane & Nair, 2005), which consist of constant 2% cambered grid sections spanwise. The design variables are the coordinates of the control points on NURBS curves in order to tailor the stiffness of the structural model. The flight case in this research is within the normal operating range for a single aisle narrow body aircraft, flight level FL310, a design cruising speed $M_c = .78$, Reynolds number $= 7.04 \times 10^6$.

4.1. *Optimisation strategy*

The design optimisation paradigm for wing roll analysis combines a parametrisation strategy by means of a CAD tool, a structural optimisation and an aerodynamic design process. Due to the complexity of the problem, this Multi-disciplinary Optimisations (MDO) paradigm is used in conjunction with a response surface approximation, as outlined in Figure 12. The programming challenges are augmented with the automated strategy of the MDO, since different solvers and solutions (structural and aerodynamic) are interdependent through numerical algorithms and convergence tolerance.

The shape parametrisation technique employed here is based on NURBS surfaces' definitions (Piegl & Tiller, 1997). It has been tailored to enhance the flexibility of such surfaces and to provide a reasonable hyperspace for the design variables. Since the planform of the wing is a priori known, only the boundary shape of the outboard section is tackled, such that a full control of the displacement field is achieved during actuation. The design space comprises mainly the interpolating points that define the bounding NURBS curves, i.e. six points for each parametrised section (i.e. crank and tip) and five points in the orthogonal direction (Ursache et al., 2011). This scheme of points is chosen to keep to the spirit of the two-dimensional approach and also to allow a large variation of the curvature of the surface, that intrinsically dictates the thickness distribution of the plate-like outboard wing.

Mapping equally spaced points from the CAD tool onto the finite element boundaries, a detailed FEA structural discretisation (Ursache et al., 2011) and the corresponding stress state of the randomly parametrised outboard patch are seen. Clearly, larger displacements can occur in the area of interest, i.e. the tip of the wing, if the bending stiffness is tailored to provide more flexibility locally, thus enhancing the stress state due to the camber cusp on the aft camber-driven profile.

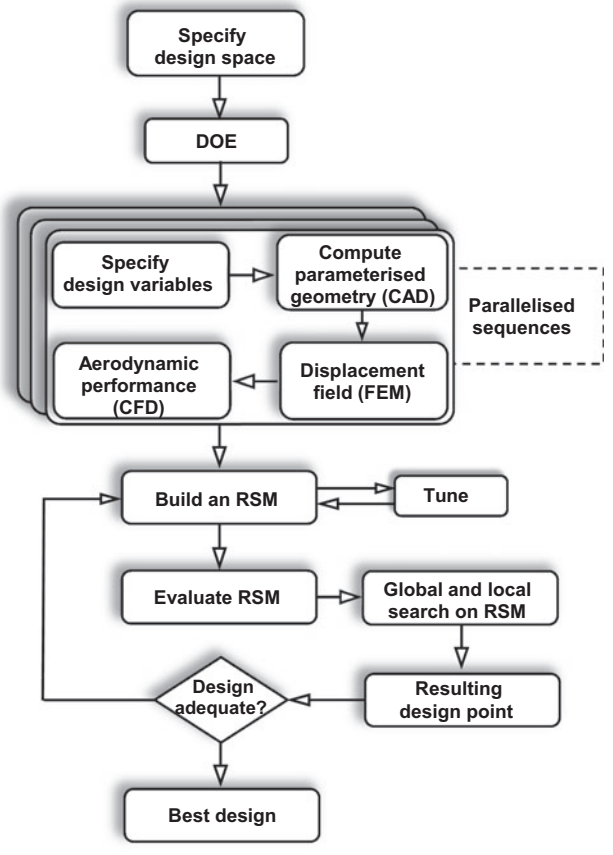

Figure 12. Optimisation strategy.

The aerodynamic characteristics of the morphing wing are provided here by VSAERO (Maskew, 1987), a panel or boundary element method which solves the linearised potential equations for inviscid, irrotational incompressible flow, with additional compressibility correction (i.e. Prandtl–Glauert and Karman–Tsien rules). The method is enhanced for boundary layer calculations, provided by a viscous potential flow coupling. The advantage of using VSAERO is that, only a surface discretisation is necessary, since it is based on a classical panel method, and does not require a grid in the flow field. The method is limited to certain flows which include relatively high Reynolds numbers and small angles of attack, applied to slim bodies with closed surfaces, up to low transonic speeds.

4.2. Response surface modelling

The MDO paradigm is based on response surface approximation, following the strategy in Figure 12. The quality of the response surface depends upon the values of the true function evaluated at sample points within the domain, often defined as *hypercube*, generated by Design of Experiments algorithms (Mead, 1998). The design optimisation process is carried out on the surface approximation so as to meet the cost functional

required. The strategy also involves an update process, where feasible solutions found on the fitted RSM to the initial data, may be fed back to the training pool for further updates and surface refinement.

Based on an $LP\tau$ array, here the Krig definition is employed (Keane & Nair, 2005) for each of the objectives and also for aerodynamics-related constraints. Previous research (Ursache et al., 2011) shows that a cost-effective approach to global approximation in such problems used a reduced form of Krig, i.e. the hyperparameters are assigned to groups of variables, rather than to each variable:

$$\mathbf{R}(\mathbf{x}_i, \mathbf{x}_j) = \exp\left[-10^{\theta}\sum_{j=1}^{k}(\|\mathbf{x}_{n+1,j} - \mathbf{x}_{i,j}\|^{p})\right] + 10^{\lambda}\delta_{ij}, \tag{19}$$

where the hyperparameter p_j can be thought of as determining the smoothness of the approximation function, θ_j can be thought of as determining the impact on the approximation function with changes of $\mathbf{x}_{n+1,j}$ with respect to $\mathbf{x}_{i,j}$.

4.3. *Pareto framework and roll augmentation*

In this study, an NSGA-II (Deb, Agrawal, Pratap, & Meyarivan, 2000) approach is used to search the parametric space built on pre-existing Krigs to find the best combinations of the design variables that can minimise the approximated functionals proposed in Equations (12)–(17). The approximation surfaces are based on sampled points from the true function. This constrained search (n.b., a Fiacco-McCormick penalty function is used (Fiacco & McCormick, 1968)) is based on a population size of 100 for 3500 generations and leads to Pareto sets of approximated designs, as shown in Figure 13, accompanied by the rank-one DoE $LP\tau$ design points from both training and predictions data-sets. In Figure 13, the three symbols, i.e. square, triangle up and triangle down are local Pareto points that perform on other fronts. Filled symbols represent the solvable points from local Pareto front with the true function. Empty symbols are the corresponding points evaluated with the true function. Some of the filled symbols (solutions) may not perform on the other Pareto fronts due to failed structural or aerodynamic analyses. The approximated solutions from the Pareto fronts are then evaluated on the true function by calling the expensive analysis codes, so as to check quantitatively and qualitatively the surface-based solutions. Since all the Pareto fronts are weak in the constitutive approximated objective space, all the points are checked with the verification scheme. This process is limited somewhat due to solver failures (i.e. structural divergence or computational issues (Ursache et al., 2006, 2011)) in the design process.

All the Pareto point designs show somewhat similar performance in terms of pressure residuals compared to target airfoils (see, for instance, Figure 14). The design point shows pressure distributions somewhat similar to flapped sections, due to increased camber line towards the wing tip which tend to shift the suction peaks towards mid chord, and lead to larger residuals with respect to the structural and aerodynamic shapes. The morphed airfoils tend to have a 'two-part' form of pressure distribution over the rear (Ursache et al., 2011), i.e. a low severity adverse pressure gradient as the trailing edge is approached, followed at $\xi \simeq .99$ by a small suction peak that indicates a sudden boundary layer separation. However, due to intrinsic tailored material fitness used in airfoil and wing optimisation, the inverse design methodology

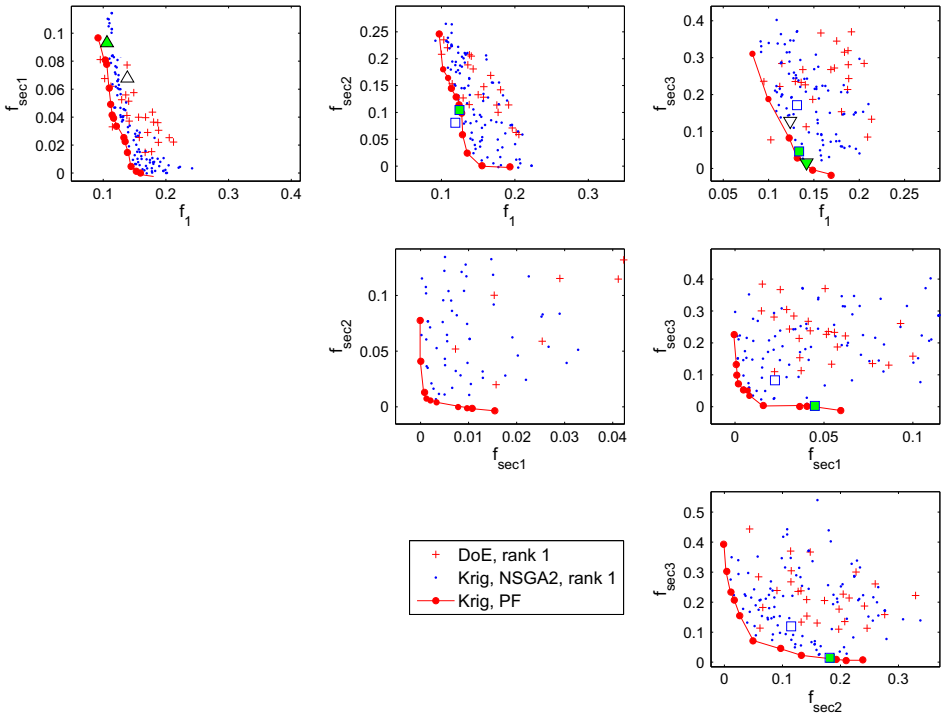

Figure 13. Reduced kriging definition, NSGA2 search, Pareto fronts.

returns better outcomes in terms of morphing airfoil and pressure distribution than previous similar research (Ursache et al., 2011).

Once Pareto points are established, morphing wing effectiveness can be assessed through a roll performance metric. These points can provide now a valid basis for comparison with a wing with conventional control surfaces (25% flap-to-wing-chord ratio) with equivalent planform definition. A number of variables i.e. equivalent aileron deflection, Mach number and angle of attack are varied to assess off-design points and generate variation curves. The aileron deployment δ is in the range of 5–20°, Mach ranges from .4 to .8 and angle of attack α from 0 to 10°. A typical Pareto design point under scrutiny is taken from objective $f_1 - f_{\text{sec }3}$, outlined in Figure 14. The results in terms of roll moment coefficient and dynamic pressure are depicted in Figure 15. Roll efficiency is computed here for one wing so as to eliminate the need to negatively morph the wing and create adverse twist that would decrease rolling moment. However, morphing-wing efficiency varies across the aileron deployment area, with better performance than classical wing with small aileron deployment (5–10°). This is due to a larger area that is deflected on morphing wing which in effect affects that wing roll. Further increasing the aileron deployment, the advantage of the morphing wing diminishes to the extent that it is outperformed by the classical wing. The residuals of datasets tend to increase with dynamic pressure and aileron deployment due to weak aerodynamic performance of NACA aft camber airfoils, but the challenge is driven by transversal shear effects of the polyfoam that ripples at high camber deflection which inherently degrades locally the lift due to non-smooth aerodynamic shape spanwise.

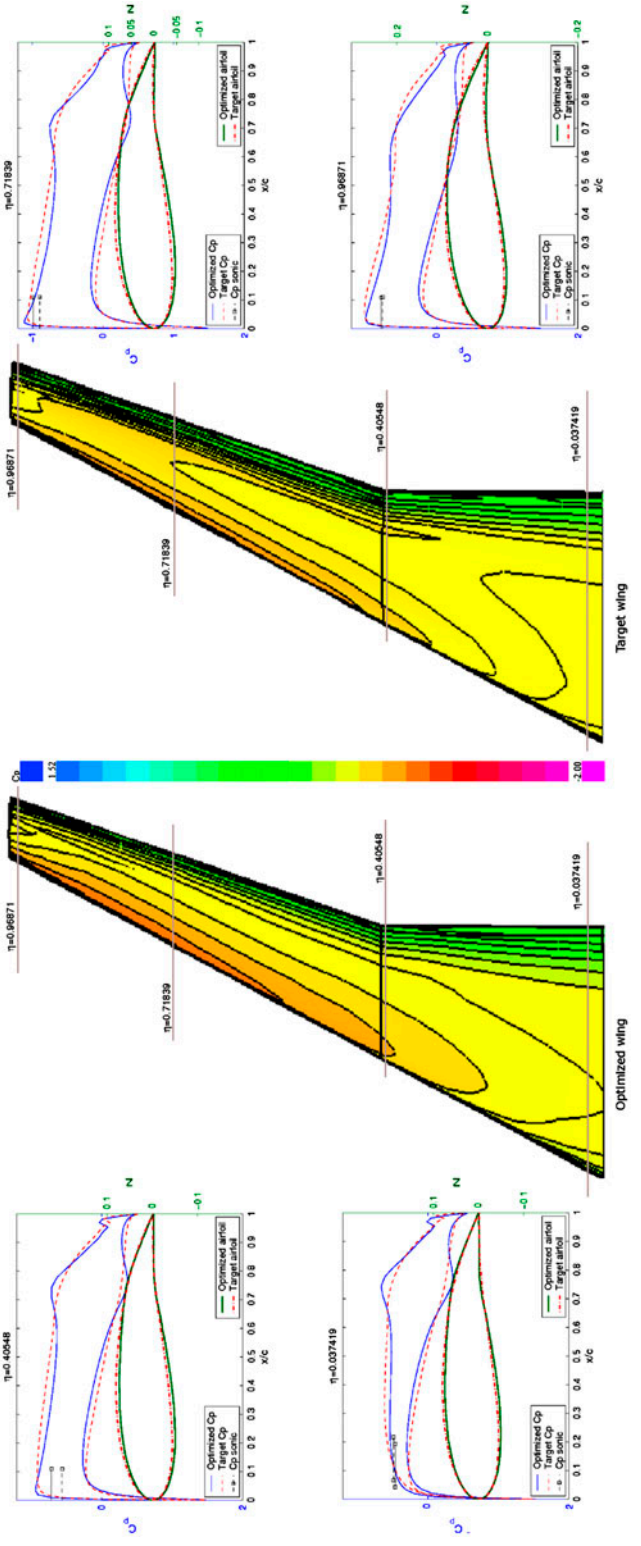

Figure 14. Pressure contours of a design-validated point (reduced Krig), Pareto front $f_1 - f_{\text{sec}\,3}$.

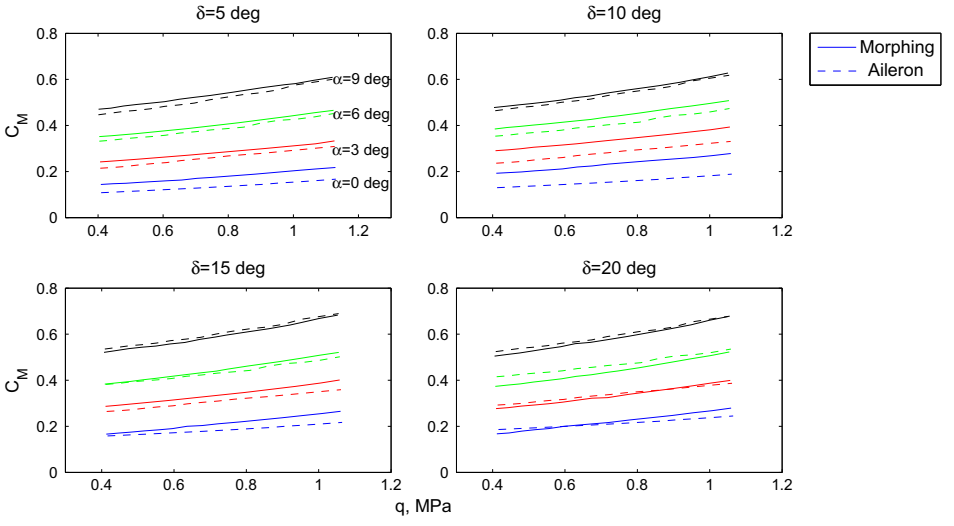

Figure 15. Roll enhancement of a design-validated point (reduced Krig), Pareto front $f_1 - f_{\sec 3}$.

The structural set-up in the optimisation scheme only ensures through constraints a smooth airfoil deflection at requisite stations and does not verify the quality of the spline function spanwise. The performance is also determined by the accuracy of the metamodels built in the initial design stage, where the correlation factor for the objectives vary between .63 and .87 (Ursache et al., 2011). Clearly, these results provide scope for further refinement of the approximation surfaces to derive the performance improvement by means of material fitness and stiffness tailoring, as well as the consideration of the adverse effect of wing twist.

5. Conclusions

A heuristic methodology to derive a global shape control for wing morphing has been presented. The design paradigm develops the key drivers for multi-shape morphing airfoils which are then used to develop an application for a fully parametrised wing shape. The wing-morphing concept is applied here to quantify enhanced roll control through a simple loading scheme that operates the structures in a post-critical regime. The optimisation strategy is twofold: it provides means for enhanced aerodynamic wing design by means of material fitness in a hierarchical multi-objective optimisation interleaving parametrisation technique with structural integrity and aerodynamic performance, and also uses approximation models combined with NSGA-II to search the Pareto front framework. The response surface used is based on a hybrid version of Krig surrogates, which showed good robustness and efficiency in terms of model fitness and computational expense.

Although the current roll efficiency results show limitations in terms of the airfoil choice and material definition, the optimisation strategy provides scope for aerodynamic shape control, enhanced by prescribed structural shapes. The design loop tackles morphing capability through modest roll control at low speeds and low angles of attack when compared to a classical wing with max 20° aileron deployment. The performance

of the wing is strictly dependent on the structural metrics and constraints, and is also related to the accuracy of the approximation model that would need further updates for additional refinement.

Nomenclature

NSGA non-dominated sorted genetic algorithm
NURBS
non-uniform rational B-splines
RMSE root mean square error
RSM response surface methodology
f objective function
f_a aerodynamic loading
f_{sec} structural related objective function
p, θ kriging hyperparameters
λ kriging regularisation constant
α angle of attack
β relaxation factor
α_i, β_i hyperelastic material parameters
μ_0 initial shear modulus
μ_i shear modulus coefficients
v_i Poisson coefficients
τ Kirchhoff stress
ϵ strain
$\mathbf{w}$ optimised displacement field
$\mathbf{w}^t$ target displacement field
C_L, C_l lift coefficient
C_D drag coefficient
$\mathbf{C_p}$ pressure coefficient
C_M roll moment coefficient
LE_{ij} component ij of logarithmic strain
N order of a hyperelastic material
s_{ij} component ij of Cauchy stress tensor
Y_{CP} y position of centre of pressure

References

Alonso, J. J., LeGresley, P., van der Weide, E., Martins, J. R., & Reuther, J. J. (2004, August 30–September 1). *A framework for high-fidelity multi-disciplinary optimization. AIAA 2004-4480*. Paper presented at the 10th AIAA/ISSMO Multidisciplany Analysis and Optimization Conference, Albany, New York.

Amitay, M., Smith, D., Kibens, V., Parekh, D., & Glezer, A. (2001). Aerodynamic flow control over an unconventional airfoil using synthetic jet actuators. *AIAA Journal, 39*, 361–370.

Barrett, R., & Vos, R. (2007). Post-buckled precompressed (PBP) subsonic micro flight control actuators and surfaces. *Proceedings of SPIE, Active and Passive Smart Structures and Integrated Systems, 6525*, 1–12. doi:10.1117/12.711561

Cai, J., & Liu, F. (2001, January 8–11). *Static aero-elastic computation with a coupled CFD and CSD method. AIAA 01-0717*. Paper presented at the 39th AIAA Aerospace Sciences Meeting and Exhibit, Reno, NV.

Deb, K., Agrawal, S., Pratap, A., & Meyarivan, T. (2000). A fast elitist non-dominated sorting algorithm for multi-objective optimization: NSGA-II. *Lecture Notes in Computer Science, 1917*, 848–849.

ESDU. (1997). *VGK method for two-dimensional aerofoil sections*. Version 2.0, 96028 B.

Fiacco, A. V., & McCormick, G. P. (1968). *Nonlinear programming: Sequential unconstrained minimization techniques*. New York, NY: Wiley.

Gibson, L. J., & Ashby, M. F. (1977). *Cellular solid structures and properties* (2nd ed.). Cambridge: Cambridge University Press.

Gilyard, G., Georgie, J., & Barnicki, J. S. (1999). *Flight test of an adaptive configuration optimization system for transport aircraft* (Tech. Rep. NASA-TM-1999-206569). Edwards, CA: Dryden Flight Research Centre.

Keane, A. J., & Nair, P. B. (2005). *Computational approaches for aerospace design*. Chicester: Wiley.

Kikuta, M. T. (2003). *Mechanical properties of candidate materials for morphing wings* (Master's thesis). Blacksburg, VA.

Lachenal, X., Weaver, P., & Daynes, S. (2012). Multi-stable composite twisting structure for morphing applications. *Proceedings of the Royal Society A: Mathematical, Physical and Engineering Sciences, 468*, 1230–1251.

Li, D., Guo, S., & Xiang, J. (2012). Modelling and nonlinear aeroelastic analysis of a wing section with morphing trailing edge. *Journal of Aerospace Engineering, 227*, 619–631. doi:10.1177/0954410012438341

Love, M. H., Zink, P. S., Stroud, R. L., Bye, D. R., & Chase, C. (2004, April 19–22). Impact of actuation concepts on morphing aircraft structures. *5th AIAA/ASME/ASCE/AHS/ASC Structures, Structural Dynamics & Materials Conference, AIAA 2004-1724*, Palm Springs, CA.

Lyn, G., & Mills, N. J. (2001). Design of foam crash mats for head impact protection. *Sports Engineering, 4*, 153–163.

Maskew, B. (1987, September). *Program VSAERO theory document. A computer program for calculating nonlinear aerodynamic characteristics of arbitrary configurations* (Contractor Report 4023). NASA.

Mead, R. (1998). *The design of experiments*. Cambridge: Cambridge University Press.

Mills, N. J., & Gilchrist, A. (2000). Modelling the indentation of low density polymer foams. *Celullar Polymers, 19*, 389–412.

Mills, N. J., & Lyn, G. (2001). Design of foam padding for rugby posts. *Proceedings of TMS Conference on Materials and Science in Sports* (pp. 105–117). San Diego.

Ogden, R. W. (1972). Large deformation isotropic elasticity: On the correlation of theory and experiment for compressible rubberlike solids. *Proceedings of the Royal Society A: Mathematical, Physical and Engineering Sciences, 328*, 567–583.

Ogden, R. W., Saccomandi, G., & Sgura, I. (2004). Fitting hyperelastic models to experimental data. *Computational Mechanics, 34*, 484–502.

Piegl, L., & Tiller, W. (1997). *The NURBS book* (2nd ed.). New York: Springer Verlag.

Pinkerton, J. L., & Moses, R. W. (1997). *A feasibility study to control airfoil shape using thunder* (Tech. Rep. NASA TM-4767). Hampton, VA: Langley Research Centre.

Rivlin, R. S. (1948). Large elastic deformations of isotropic materials. I. Fundamental concepts. *Philosophical Transactions of the Royal Society A: Mathematical, Physical and Engineering Sciences, 240*, 459–490.

Rodrigues, A. R. (2007, January 8–11). Morphing aircraft technology survey. *45th AIAA Aerospace Sciences Meeting and Exhibit, AIAA 2007-1258*, Reno, Nevada.

Roth, B. D., & Crossley, W. A. (2003, November 17–19). Application of optimization techniques in the conceptual design of morphing aircraft. *AIAA's 3rd Annual Aviation Technology, Integration and Operations (ATIO) Tech, AIAA 2003-6733*, Denver, CO.

Saggere, L., & Kota, S. (1999). Static shape control of smart structures using compliant mechanisms. *AIAA Journal, 37*, 572–578.

Scherer, L. B., Martin, C. A., Appa, K., Kudva, J. N., & West, M. N. (1997). Smart wing test results. *SPIE Proceedings, 3044*, 1–11.

Schrodt, M., Benderoth, G., Kühhorn, A., & Silber, G. (2005). Hyperelastic description of polymer soft foams at finite deformations. *Technische Mechanik, 25*, 162–173.

Seifert, A., Eliahu, S., Greenblatt, D., & Wygnanski, I. (1998). Use of piezoelectric actuators for airfoil separation control. *AIAA Journal, 36*, 1535–1537.

Smith, M. J., Hodges, D. H., & Cesnik, C. E. S. (1995, November). *An evaluation of computational algorithms to interface between CFD and CSD methodologies* (Tech. Rep. WL-TR-96-3055). USAF Wright Laboratories.

Thomson, R. D., Birkbeck, A. E., Tan, W. L., McCafferty, L. F., Grant, S., & Wilson, J. (1999). The modelling and performance of training shoe cushioning systems. *Sports Engineering, 2*, 109–120.

Thuwis, G. (2012, June). *Stiffness and layout tailoring of a morphing high-lift system with aeroelastic loads* (Ph.D. thesis). Delft University.

Thuwis, G. A. A., Abdalla, M. M., & Gurdal, Z. (2010). Optimization of a variable-stiffness skin for morphing high-lift devices. *Smart Materials and Structures, 19*, 1–10. doi:10.1088/0964-1726/19/12/124010

Twizell, E. H., & Ogden, R. W. (1983). Non-linear optimization of the material constants in Ogden's stress-deformation function for incompressinle isotropic elastic materials. *The Journal of the Australian Mathematical Society. Series B. Applied Mathematics, 24*, 424–434.

Ursache, N., Bressloff, N., & Keane, A. J. (2004, July). The design of post-buckled spinal structures for airfoil shape control using optimization methods. *5th ASMO UK/ISSMO Conference on Engineering Design Optimization*, Stratford-upon-Avon: Leeds University Press.

Ursache, N., Bressloff, N., & Keane, A. J. (2011). Aircraft roll enhancement via multi-objective optimization using surrogate modeling. *AIAA Journal, 49*, 1525–1541. doi:10.2514/1.J050812.

Ursache, N., Keane, A. J., & Bressloff, N. W. (2006). Design of postbuckled spinal structures for airfoil camber and shape control. *AIAA Journal, 44*, 3115–3124. doi:10.2514/1.22636.

Ursache, N., & Mares, C. (2012, April 23–26). Optimisation of a corrugated skin for a morphable winglet. *53rd AIAA/ASME/ASCE/AHS/ASC Structures, Structural Dynamics, and Materials Conference*. Honolulu, HI: AIAA.

Ursache, N., Melin, T., Isikveren, A. T., & Friswell, M. (2007, September 18–20). Morphing winglets for aircraft multi-phase improvement. *7th AIAA Aviation Technology, Integration and Operations Conference (ATIO)*. Belfast, Northern Ireland: AIAA.

Voracek, D., Pendleton, E., Reichenbach, E., Griffin, K., & Welch, L. (2003). *The active aeroelastic wing phase I flight research through January 2003* (Tech. Rep. NASA-TM-2003-210741). Dryden Flight Research Centre.

Weisshaar, T. (2006). Morphing aircraft technology – New shapes for aircraft design. *Multifunctional Structures / Integration of Sensors and Antennas*. RTO-MP-AVT-141, Neuilly-sur-Seine. France: RTO.